

INSTABILITIES IN PLUG-AND-PLAY (PNP) ALGORITHMS FROM A LEARNED DENOISER

ABINASH NAYAK

ABSTRACT. It's well-known that inverse problems are ill-posed and to solve them meaningfully, one has to employ regularization methods. Traditionally, popular regularization methods are the penalized Variational approaches. In recent years, the classical regularization approaches have been outclassed by the so-called plug-and-play (PnP) algorithms, which copy the proximal gradient minimization processes, such as ADMM or FISTA, but with any general denoiser. However, unlike the traditional proximal gradient methods, the theoretical underpinnings, convergence, and stability results have been insufficient for these PnP-algorithms. Hence, the results obtained from these algorithms, though empirically outstanding, can't always be completely trusted, as they may contain certain instabilities or (hallucinated) features arising from the denoiser, especially when using a pre-trained learned denoiser. In fact, in this paper, we show that a PnP-algorithm can induce hallucinated features, when using a pre-trained deep-learning-based (DnCNN) denoiser. We show that such instabilities are quite different than the instabilities inherent to an ill-posed problem. We also present methods to subdue these instabilities and significantly improve the recoveries. We compare the advantages and disadvantages of a learned denoiser over a classical denoiser (here, BM3D), as well as, the effectiveness of the FISTA-PnP algorithm vs. the ADMM-PnP algorithm. In addition, we also provide an algorithm to combine these two denoisers, the learned and the classical, in a weighted fashion to produce even better results. We conclude with numerical results which validate the developed theories.

1. Introduction

1.1. Inverse Problems and Regularization: Mathematically, an inverse problem is often expressed as the problem of estimating a (*source*) \hat{x} which satisfies, for a given (*effect*) b , the following matrix (or operator) equation

$$A\hat{x} = b, \tag{1.1}$$

where the matrix $A \in \mathbb{R}^{n \times m}$ and the vectors $\hat{x} \in \mathbb{R}^n$, $b \in \mathbb{R}^m$ are the discrete approximations of an infinite dimensional model, describing the underlying physical phenomenon. The inverse problem (1.1) is usually ill-posed, in the sense of violating any one of the Hadamard's conditions for well-posedness: (i) Existence of a solution (for b not in the range of A), (ii) uniqueness of the solution (for non-trivial null-space of A) and, (iii) continuous dependence on the data (for ill-conditioned A). Conditions (i) and (ii) can be circumvented by relaxing the definition of a solution for (1.1), for example, finding the least square solution or the minimal norm solution

Date: September 6, 2021.

2020 Mathematics Subject Classification. Primary 65K05, 65K10; Secondary 65R30, 65R32.

Key words and phrases. Inverse problems, Ill-posed problems, Regularization, Variational minimization, Numerical methods, Plug-and-Play (PnP), BM3D denoiser, Computed tomography.

(i.e., the pseudo-inverse solution x^\dagger). The most (practically) significant condition is condition-(iii), since failing of this leads to an absurd (unstable) solution. That is, for an (injective) A and an exact b (noiseless), the solution of (1.1) can be approximated by the (LS) least-square solution (x^\dagger), i.e., x^\dagger is the minimizer of the following least-square functional

$$F(x) = \|Ax - b\|_2^2, \quad (1.2)$$

where as, for a noisy data b_δ (which is practically true, most of the time) such that $\|b - b_\delta\| \leq \delta$, the simple least-square solution x_δ^\dagger , with respect to b_δ in (1.2), fails to approximate the true solution, i.e., $\|x_\delta^\dagger - x^\dagger\| \gg \delta$, which in turn implies, $\|x_\delta^\dagger - \hat{x}\| \gg \delta$, due to the ill-posedness of the inverse problem (1.1). To counter such instabilities or ill-posedness of inverse problems, regularization methods have to be employed.

1.2. Variational (or penalized) regularization and Related works.

Such approaches, also known as Tikhonov-type regularization, are probably the most well known regularization techniques for solving linear, as well as nonlinear, inverse problems (see [1, 2, 3, 4, 5]), where, instead of minimizing the simple least-square functional (1.2), one minimizes a penalized (or constrained) functional:

$$F(x; \mathcal{D}, \lambda, \mathcal{R}) = \mathcal{D}(Ax, b_\delta) + \lambda \mathcal{R}(x), \quad (1.3)$$

where \mathcal{D} is called the data-fidelity term (imposing data-consistency), \mathcal{R} is the regularization term (imposing certain structures, based on some prior knowledge of the solution \hat{x}) and, $\lambda \geq 0$ is the regularization parameter that balances the trade-off between them, depending on the noise level δ , i.e., $\lambda = \lambda(\delta)$. The formulation (1.3) also has a Bayesian interpretation, where the minimization of $F(x; \mathcal{D}, \lambda, \mathcal{R})$ corresponds to the maximum-a-posteriori (MAP) estimate of \hat{x} given b_δ , where the likelihood of b_δ is proportional to $\exp(-\mathcal{D}(x))$ and the prior distribution on \hat{x} is proportional to $\exp(-\mathcal{R}(x))$. Classically, $\mathcal{D}(Ax, b_\delta) = \|Ax - b_\delta\|_p^p$ and $\mathcal{R}(x) = \|Lx - \bar{x}\|_q^q$, where L is a regularization matrix, with the null spaces of A and L intersecting trivially, and p, q determine the involved norms. For large scale problems, the minimization of (1.3) is done iteratively, and for convex, differentiable functions \mathcal{D} and \mathcal{R} , one can minimize (1.3) either via the simple steepest descent method or via faster Krylov subspace methods, such as Conjugate-Gradient method etc., see [6, 7, 8, 1]. Where as, for a non-differentiable \mathcal{R} , which is proper, closed and convex, the non-differentiability issue can be circumvented by using a proximal operator, see [9, 10, 11] and references therein, which is defined as

$$\text{Prox}_{\lambda \mathcal{R}}(v) = \arg \min_x \lambda \mathcal{R}(x) + \frac{1}{2} \|x - v\|_2^2. \quad (1.4)$$

Basically, for smooth $\mathcal{D}(x)$ and non-smooth $\mathcal{R}(x)$, the minimization problem corresponding to (1.3) can be solved via two first-order iterative methods:

- (1) Forward-backward splitting (FBS), also known as Iterative shrinkage/soft thresholding algorithm (ISTA) and has a faster variant Fast ISTA (FISTA), where each minimization step is divided into two sub-steps, given by

$$z_{k+1}^\delta = x_k^\delta - \tau_k \nabla_x \mathcal{D}(x_k^\delta) \quad \leftarrow \text{data-consistency step} \quad (1.5)$$

$$x_{k+1}^\delta = \text{Prox}_{\lambda \tau_k \mathcal{R}}(z_{k+1}^\delta) \quad \leftarrow \text{data-denoising step} \quad (1.6)$$

where $\tau_k \geq 0$ is the step-size at the k^{th} iteration.

- (2) Alternating direction method of multipliers (ADMM), where three sequences are alternatively updated as follows,

$$x_{k+1}^\delta = \text{Prox}_{\frac{1}{\rho}\mathcal{D}}(z_k^\delta - u_k^\delta) \leftarrow \text{data-consistency step} \quad (1.7)$$

$$z_{k+1}^\delta = \text{Prox}_{\frac{\lambda}{\rho}\mathcal{R}}(x_{k+1}^\delta + u_k^\delta) \leftarrow \text{data-denoising step} \quad (1.8)$$

$$u_{k+1}^\delta = u_k^\delta + x_{k+1}^\delta - z_{k+1}^\delta, \leftarrow \text{noise update step} \quad (1.9)$$

where $\rho > 0$ is the Lagrangian parameter, which only effects the speed of convergence and not the solution (minimizer) of (1.3).

From the above two expressions, one can observe that, each method comprises of two fundamental steps: (1) data-consistency, and (2) data-denoising. This motivated, authors in [12], to replace the $\text{Prox}_{\delta\mathcal{R}}$ operator in the denoising step of ADMM by an off-the-shelf denoiser H_σ , which is tuned to $H_{\delta=\sigma/\rho}$, where σ is the denoising strength of the original denoiser H_σ , and termed the process as the PnP-algorithm (plug-and-play method). However, note that, once the proximal operator is replaced by any general denoiser then the Variational problem (1.3) breaks down, as not all denoisers can be expressed as a proximal operator of some function \mathcal{R} . Hence, all the theories and results related to the classical Variational regularization methods also break down, such as the convergence, regularization and stability analysis, and even, the meaning of the solution, i.e., how to define the obtained solution? is it a minimizer of some functional? etc. Though empirical results show the convergence of these PnP-algorithms, there is no proof of it, for any general denoisers. However, under certain assumptions and restrictions (such as boundedness, nonexpansiveness, etc.) on the denoiser, there have been some convergence proof, see [13, 14, 15, 16, 17] and references therein. There are also some other variants of such PnP-methods, such as Regularization by Denoising (RED)[18], Regularization by Artifact-Removal (RARE) [19], etc.

Contribution of this paper.

- In this paper, we present the instabilities arising in such PnP-algorithms, due to the lack of theoretical underpinnings, especially for an off-the-shelf non-classical denoisers, such as, a deep-learning based denoiser.
- We also present certain regularization methods to subdue the above mentioned instabilities, which leads to much better and stable recoveries.
- We also compare the FBS-PnP algorithm with the ADMM-PnP algorithm and show the advantages/disadvantages of one over the other, i.e., which algorithm is more appropriate for a given denoiser. Note that, in the classical scenario, both these algorithms produce the same result, which is the minimizer of the functional defined in (1.3). However, for PnP algorithms with general denoisers, they are not the same, i.e., the architecture of the iterative process does effect the recovered solution.
- We also provide methods to combine these two denoisers, the classical and the learned, in a weighted manner, which take advantages of both these worlds and produce better results.
- We conclude with numerical examples, validating the developed theories.

2. PNP-ALGORITHMS AS STRUCTURED ITERATIONS

In this section, we interpret PnP-algorithms from a different perspective. First, let's rewrite the PnP-versions, for any general denoiser H_σ , from their respective classical proximal gradient methods, i.e.,

- (1) **FBS-PnP (Forward-backward splitting - PnP)**: In this algorithm, for a fixed denoiser H_σ (of denoising strength corresponding to noise level σ) and starting from an initial choice z_0^δ , at any iteration step $k \geq 1$, we have

$$z_{k-1}^\delta \mapsto x_k^\delta = z_{k-1}^\delta - \tau_k \nabla_x \mathcal{D}(z_{k-1}^\delta) \quad \leftarrow \text{data-consistency step} \quad (2.1)$$

$$x_k^\delta \mapsto z_k^\delta = H_{\sigma_k}(x_k^\delta), \quad \leftarrow \text{data-denoising step}, \quad (2.2)$$

where H_{σ_k} is the updated kth denoiser, with the denoising strength corresponding to $\sigma_k = \tau_k \sigma$.

- (2) **ADMM-PnP (Alternating direction method of multipliers - PnP)**: Here, for a fixed denoiser H_σ (of denoising strength corresponding to noise level σ) and starting from initial choices x_0^δ , z_0^δ and u_0^δ , at any iteration step $k \geq 1$, we have

$$\begin{aligned} x_{k+1}^\delta &= \text{Prox}_{\frac{1}{\rho} \mathcal{D}}(z_k^\delta - u_k^\delta) \quad \leftarrow \text{data-consistency step} \quad (2.3) \\ &= \arg \min_x \mathcal{D}(x) + \rho \|x - (z_k^\delta - u_k^\delta)\|_2^2 \end{aligned}$$

$$z_{k+1}^\delta = H_{\sigma_k}(x_{k+1}^\delta + u_k^\delta) \quad \leftarrow \text{data-denoising step} \quad (2.4)$$

$$u_{k+1}^\delta = u_k^\delta + x_{k+1}^\delta - z_{k+1}^\delta \quad \leftarrow \text{noise update step} \quad (2.5)$$

where H_{σ_k} is the kth updated denoiser, with the denoising strength corresponding to $\sigma_k = \frac{\sigma}{\rho}$.

Note that, for the classical case (H_{σ_k} corresponding to a closed, proper and convex regularizer \mathcal{R} in (1.3)), both the above algorithms should produce the same result, the minimizer of (1.3), and the parameters values, τ_k and ρ , only effect the convergence of the algorithms and not the final solution, $x^\delta(\mathcal{D}, \lambda, \mathcal{R})$. However, this might not be true for PnP algorithms, when using any general denoiser H_σ .

Also, note that, the resulting direction at $(k-1)^{th}$ step, in the FBS-PnP algorithm, is given by

$$\begin{aligned} d_{k-1}^\delta &:= z_k^\delta - z_{k-1}^\delta \quad (2.6) \\ &= \underbrace{-\tau_k \nabla_x \mathcal{D}(z_{k-1}^\delta)}_{\text{data-consistency}} + \underbrace{(H_{\sigma_k}(x_k^\delta) - x_k^\delta)}_{\text{data-denoising}}, \end{aligned}$$

and the direction d_{k-1}^δ , as defined in (2.6), will be a descent direction provided it satisfies, for $\mathcal{D}(x) = \|Ax - b_\delta\|_2^2$,

$$\left(d_k^\delta, -\nabla_x \mathcal{D}(x_k^\delta) \right)_2 = \left(d_k^\delta, -A^*(Ax_k^\delta - b_\delta) \right)_2 > 0, \quad (2.7)$$

where $(\cdot, \cdot)_2$ is the associated ℓ_2 -product. This can be achieved for H_{σ_k} satisfying

$$\|H_{\sigma_k}(x_k^\delta) - x_k^\delta\| < \|-\tau_k \nabla_x \mathcal{D}(x_{k-1}^\delta)\|, \quad (2.8)$$

since then

$$\left(d_{k-1}^\delta, -\tau_k \nabla_x \mathcal{D}(z_{k-1}^\delta) \right)_2 \geq \tau_k \|\nabla_x \mathcal{D}(z_{k-1}^\delta)\| (\tau_k \|\nabla_x \mathcal{D}(z_{k-1}^\delta)\| - \|H_{\sigma_k}(x_k^\delta) - x_k^\delta\|) > 0.$$

Therefore, for such descent directions d_{k-1}^δ , the relative errors in the recovery process will follow a semi-convergent trail, and hence, one can recover a regularized solution (via early stopping) containing certain structures in it, which are imposed by the denoiser H_{σ_k} , for further details see [20]. In other words, for directions d_k^δ satisfying (2.8), we obtain a family of regularized solutions given by

$$\begin{aligned} \mathcal{I}_3 := \{ & x^\delta(\mathcal{D}, k, d_k^\delta; \mathcal{S}) : x_k^\delta = x_{k-1}^\delta + d_{k-1}^\delta, \quad 1 \leq k \leq k(\delta, \mathcal{S}) \leq \infty, \\ & \text{s.t. } \left(d_{k-1}^\delta, -\tau_{k-1} \nabla_x \mathcal{D}(x_{k-1}^\delta) \right)_2 > 0 \text{ and } \mathcal{S} \text{ is a selection criterion.} \}. \end{aligned} \quad (2.9)$$

Note that, (2.8) is only a sufficient condition for d_k^δ to be a descent direction, i.e., d_k^δ violating (2.8) can also be a descent direction (satisfying (2.7)). In fact, d_k^δ need not even satisfy (2.7) for all values of k , i.e., d_k^δ doesn't need to be a descent direction for all $k \geq 1$, in which case, we obtain a family of regularized solutions given by

$$\begin{aligned} \mathcal{I}_5 := \{ & x^\delta(\mathcal{D}, k, d_k^\delta, x_0^\delta; \mathcal{S}) : x_k^\delta = x_{k-1}^\delta + d_{k-1}^\delta, \text{ starting from } x_0^\delta, \\ & \text{s.t. } d_{k-1}^\delta \text{ satisfies (2.11) and } \mathcal{S} \text{ is a selection criterion.} \}, \end{aligned} \quad (2.10)$$

where the condition (2.11) is a generalization of (2.7), given by,

$$\begin{aligned} \left(d_k^\delta, -\nabla_x \mathcal{D}(x_k^\delta) \right)_2 &> 0, \quad \text{for } \mathcal{D}(x_k^\delta) > \epsilon_2(\delta) \text{ or } k \leq k(\delta), \text{ and} \\ \mathcal{D}(x_k^\delta + d_k^\delta) &\geq \epsilon_1(\delta), \quad \text{for } \mathcal{D}(x_k^\delta) \leq \epsilon_2(\delta) \text{ or } k > k(\delta). \end{aligned} \quad (2.11)$$

With the above formulation for the family of regularized solutions, it can be shown that the solution of an ADMM-PnP algorithm falls in the class \mathcal{I}_5 , see [20] for details.

Also, in the recovery process, the dynamics of the denoising is reflected in the denoising-to-consistency ratio, which is defined as follows

$$DC(k) := \frac{\|H_{\sigma_k}(x_k^\delta) - x_k^\delta\|}{\|-\tau_k \nabla_x \mathcal{D}(x_{k-1}^\delta)\|} = \frac{\|H_{\sigma_k}(x_k^\delta) - x_k^\delta\|}{\|x_k^\delta - x_{k-1}^\delta\|}. \quad (2.12)$$

That is, if the ratio is very small $DC(k) \ll 1$, then the extent of denoising is very small in comparison to the amount of improvement towards the noisy data, and hence, can be lead to a noisy recovery. Where as, if the ratio is very large $DC(k) \gg 1$, then the extent of denoising is also very large, relative to the improvement in the data-consistency step, and hence, can lead to an over-smoothed solution. However, this doesn't always means that for $DC(k) \ll 1$ or $DC(k) \gg 1$, the recoveries will be too noisy or over-smoothed, respectively, since, if the noise levels in b_δ is low (i.e., $\|x_k^\delta - x_{k-1}^\delta\|$ can be large) and the noise in x_k^δ is small (i.e., $\|H_{\sigma_k}(x_k^\delta) - x_k^\delta\|$ can be small), then $DC(k) \ll 1$, but can still produce well-denoised iterate z_k^δ ; on the other hand, if H_{σ_k} is an excellent denoiser (i.e., $\|H_{\sigma_k}(x_k^\delta) - \hat{x}\| \ll 1$, where \hat{x} is the true solution), then, even for high noise levels in x_k^δ and b_δ , the ratio $DC(k) \gg 1$ and one can still produce excellent recovery. Nevertheless, inspecting the ratio $DC(k)$ provides some insights regarding the denoising dynamics in the recovery process, and thus, can help to improve the recovery in certain cases, details in §3.

2.1. Classical Denoiser vs. Learned Denoiser:

Note that, a classical denoiser H_σ is dependent on a denoising parameter ($\sigma \geq 0$), which controls the denoising strength of the denoiser, i.e., larger σ implies stronger denoising and vice-versa. Therefore, the parameter σ needs to appropriately tuned,

based on the noise level δ , for an effective denoising, i.e., one cannot use H_σ , for a fixed σ , universally for any noise level δ . In contrast, “an ideally learned denoiser” H_{θ_0} can be used to denoise universally, where an ideally learned denoiser implies, H_{θ_0} has learned to denoise at an universal level, i.e., noises of all levels and distributions. Here, $\theta_0 \in \mathbb{R}^d$, for some d (usually, high dimension), denotes the pre-trained internal parameters of the learned denoiser, such as the weights of a neural network. Of course, an ideally learned denoiser only exists in a hypothetical setting. In a typical scenario, one has a set of learning examples (training data) and a denoising architecture H_θ is trained on that data set, i.e., the parameters (θ) of the denoiser H_θ is optimized to θ_0 such that H_{θ_0} yields the “most effective denoising” on that data set, where the “most effective denoising” depends on the performance measuring metric (loss function) and the optimization process. Then, one hopes that for examples outside the training data set (i.e., in the testing data set) H_{θ_0} will also perform effective denoising. Hence, one can see that, when using a parameter-dependent classical denoiser H_σ , for solving an inverse problem, the denoising parameter σ can also serve as a regularization parameter, which can be tuned appropriately for different noise levels δ . Where as, when using a pre-trained learned denoiser H_{θ_0} , whose internal parameters have been already optimized, one hopes that the bag of training examples contains noises of different levels and distributions, suited for that inverse problem. Now, even with a set of proper training examples, it is shown in [21] that recovery algorithms for inverse problems based on deep learning can be very unstable, as a result of adversarial attacks. Although, the structure of the recovery processes mentioned there is of slightly different flavor than that of a PnP-algorithm with (deep) learned denoiser.

In this paper, we consider a pre-trained deep learning based denoiser H_{θ_0} , more specifically a pre-trained DnCNN network for denoising, and compare the recoveries obtained using it with the recoveries obtained using a classical denoiser H_σ (here, BM3D denoiser). To have a fairer comparison, we even fixed the denoising strength of the classical denoiser, i.e., we don’t tune the parameter σ for an effective denoising or regularizing the recovered solution of the inverse problem, rather, we use a fixed the denoiser H_{σ_0} for the recovery process. Furthermore, we even chose a weaker denoiser (i.e., smaller σ value) so as to compare the instabilities in the recovered solutions, arising from a weak classical denoiser H_{σ_0} vs. a strong learned denoiser H_{θ_0} , i.e., the difference between the lack of adequate (classical) denoising vs. denoising based on some prior learning. We also compare the recoveries obtained using different iterative processes, i.e., the FBS-PnP vs. the ADMM-PnP algorithm, based on the classical denoiser H_{σ_0} and the learned denoiser H_{θ_0} . In other words, we show that, not only the denoisers, but also the nature of the iterative flow (even for the same denoiser) significantly influence the efficiency of the recovery process, which is not the case for traditional proximal operators, that are based on some regularization function \mathcal{R} in (1.3).

In addition, we also present techniques to subdue the instabilities arising from these denoisers, for an effective recovery. It is shown that, for stronger denoisers (be it a classical or learned denoiser), the ADMM-PnP algorithm is more effective than the FBS-PnP algorithm, where as, for a weaker denoiser, the FBS-PnP algorithm is better than the ADMM-PnP algorithm, as in the FBS-PnP method the data-consistency steps are improved gradually, and hence, a weaker denoiser can denoise the creeping noise effectively, in contrast, for a stronger denoiser, the FBS-PnP

algorithm will easily over-smooth the recovery process, and in this case, the ADMM-PnP algorithm is much more effective. These statements are (empirically) validated via numerical and computational examples in the following section.

3. NUMERICAL EXAMPLES

In this section, we present certain computational results to validate the reasoning provided in the previous sections. Note that, the goal here is to compare the recoveries obtained using a pre-trained learned denoiser H_{θ_0} and a fixed classical denoiser H_{σ_0} , corresponding to the FBS-PnP and ADMM-PnP algorithm. Hence, we don't repeat the experiments over and over to fine tune the denoising parameters θ and/or σ , respectively, to produce the optimal results, rather, for the fixed θ_0 and σ_0 , we study the instabilities arising from these denoisers and suggest appropriate measures to subdue them and improve the recovery process.

All the experiments are computed in MATLAB, where we consider the classical denoiser H_{σ_0} as the BM3D denoiser with $\sigma_0 = 0.001$, and the MATLAB code for the BM3D denoiser is obtained from <http://www.cs.tut.fi/foi/GCF-BM3D/>, which is based on [22, 23]. Here, we kept all the attributes of the code in their original (default) settings and assign the denoising strength $\sigma = 0.001$, as the standard deviation of the noise, when denoising x_k^δ iterates to z_k^δ . And for the learned denoiser H_{θ_0} , we used MATLAB's pre-trained DnCNN denoiser, the details of which (such as the number of layers, optimization procedures etc.) can be found in <https://www.mathworks.com/help/images/ref/denoisingnetwork.html>. First, to compare the effectiveness of their denoising abilities, we implement them on noisy Shepp-Logan phantom for different noise levels and the results are shown in Figure 1, where σ_δ denotes the standard deviation of the additive Gaussian noise with zero-mean. Observe that, the denoising ability of the learned denoiser H_{θ_0} is very impressive overall, irrespective of the noise levels, whereas, the denoising from the classical denoiser H_{σ_0} is (practically) negligible for all noise levels. Also, note that, when the noise level (σ_δ) decreases, the performance metrics of H_{θ_0} (as well as H_{σ_0} , though insignificantly) increases, however, there is a noticeable difference in the dynamics of different evaluation metrics, such as, the PSNR values of the noisy data x_{σ_δ} (for smaller σ_δ values) are even better than that of the (learned) denoised image $H_{\theta_0}(x_{\sigma_\delta})$, whereas, the SSIM values follow a completely different trail for different noise levels, it's always better than the others. Such discrepancies reflect that the denoiser H_{θ_0} has been trained (or has learned) to emphasize certain features/structures of denoising, over certain others, and hence, can be susceptible to hallucinate (or impose) those features, leading to instabilities (or generating artifacts) that are quite different in nature than the instabilities (or noises) arising from the inherent ill-posedness of the inverse problems, which are reflected in the following examples. In all of the following examples, when the FBS-PnP algorithm is implemented, we consider the step-size to be $\tau = 10^{-5}$ (a constant step-size), unless otherwise stated, and the relative noise levels in the data $\left(\frac{\|b_\delta - b\|}{\|b\|}\right)$, the number of iterations, the Lagrangian parameter (ρ) value, when using ADMM-PnP algorithm, etc. are specified in the example settings. The data-consistency term is considered to be $\mathcal{D}(x) = \|Ax - b_\delta\|_2^2$ and the selection criterion \mathcal{S}_0 , for the regularized solution, is considered to be the cross validation criterion, for some leave-out set of the noisy data b_δ (which is 1% of b_δ). The numerical values, corresponding to the recovered solutions, are shown in Tables 1, 2, 3 and 4, where MSE denotes the mean-squared

error (calculated as $\frac{\|x_\delta - x\|}{\|x\|}$), PSNR stands for the peak signal-to-noise ratio in dB (computed using MATLAB’s inbuilt function $psnr(x_\delta, x)$), SSIM stands for the structure similarity index measure (which is again computed using MATLAB’s inbuilt routine $ssim(x_\delta, x)$), ‘ \mathcal{D} -err.’ stands for the discrepancy error $\left(\frac{\|Ax_k^\delta - b_{D,\delta}\|_2}{\|b_{D,\delta}\|_2}\right)$ and ‘ \mathcal{S} -err.’ stands for the cross-validation error $\left(\frac{\|Ax_k^\delta - b_{S,\delta}\|_2}{\|b_{S,\delta}\|_2}\right)$, where $b_{S,\delta} \subset b_\delta$ is the left-out set and $b_{D,\delta} = b_\delta \setminus b_{S,\delta}$, and the recoveries are shown in Figures 2, 3 and 7.

In the following examples, the matrix equation (1.1) corresponds to the discretization of a radon transformation, which is associated with the X-ray computed tomography (CT) reconstruction problem, where we generate the matrix $A \in \mathbb{R}^{m \times n}$, $\hat{x} \in \mathbb{R}^n$ and $b \in \mathbb{R}^m$ from the MATLAB codes presented in [24]. The dimension n corresponds to the size of a $N \times N$ image, i.e., $n = N^2$, and the dimension m is related to the number of rays per projection angle and the number of projection angles, i.e., $m = M_1 \times M_2$, where M_1 implies the number of rays/angle and M_2 implies the number of angles.

Example 3.1. [Fast FBS-PnP using H_{θ_0} vs. H_{σ_0}]

In this example, we compare the recoveries obtained in the Fast FBS-PnP algorithm, when using a learned denoiser H_{θ_0} vs. when using a classical denoiser H_{σ_0} . We present the nature of instabilities arising from a learned denoiser H_{θ_0} , when used in a FBS-PnP algorithm, and provide a technique to subdue them. Here, for the true phantom, we consider the standard (256×256) Shepp-Logan phantom ($\hat{x} \in \mathbb{R}^{65536}$ and $\hat{x}_i \in [0, 1]$). However, during the recovery process, we do not enforce the constraint $x_i \geq 0$ on the iterates, since the motive is to compare the efficiency of these two denoisers, while solving an inverse problem, independent of any constraints. The matrix $A \in \mathbb{R}^{43440 \times 65536}$ is generated using the $PRtomo()$ code from [24], corresponding to a ‘fancurved’ CT problem with only 120 view angles (which are evenly spread over 360°). The noiseless data is generated by $b := A\hat{x} \in \mathbb{R}^{43440(=362 \times 120)}$, which is then contaminated by additive Gaussian noise of zero-mean to produce noisy data b_δ such that the relative error is around 1%. We leave out 1% of the noisy data b_δ for generating the cross-validation errors (the selection criterion \mathcal{S}_0) during the iterative process and consider a constant step-size $\tau = 10^{-5}$. The iterations are terminated if the cross-validation errors start increasing steadily and continuously, after allowing certain number of small fluctuations, or if the iterations have reached the maximum limit (250 iterations), unless otherwise stated. The numerical values corresponding to the recoveries are shown in Table 1 and figures in Figure 2.

Note that, Figure 2a shows the recovered solution without using any denoisers, i.e., the solution after 250 Conjugate-Gradient Least-Squares (CGLS) iterations, and one can notice the noisy texture in the image and certain artifacts arising from the ill-posedness of the problem. Where as, Figure 2c shows the regularized solution ($x_{k(\delta, \mathcal{S}_0)}^\delta$, for $k(\delta, \mathcal{S}_0) = 47$) when using the learned denoiser H_{θ_0} , where the nature of instabilities (or artifacts) are quite different than that in Figure 2a, without any denoiser. The reason being, as is explained above, the learned denoiser H_{θ_0} has learned certain features/structures to impose on the images, which it considers as denoising, especially for images with lower noise levels. And, in a Fast FBS-PnP algorithm, the iterates x_k^δ are improved gradually to fit the (noisy) data b_δ , implying that the initial iterates are less noisy, and hence, H_{θ_0} imposes certain structures

to them, which are then transformed into corrupted artifacts over later iterations. Where as, in an ADMM-PnP algorithm the iterates x_k^δ approximates the noisy LS-solution x_δ^\dagger very rapidly (for smaller values of the Lagrangian parameter ρ), and thus, the iterates are heavily contaminated with noise arising from the noisy data (b_δ), which then can be effectively denoised by H_{θ_0} , see Example 3.2.

In addition, note that, if the iterations were not terminated at $k(\delta, \mathcal{S}_0)$, then the relative error in the recovered solution for the last iterate (x_N^δ) would be enormous, i.e., the relative errors in the recovery process have a semi-convergence nature, see Figure 2g and 2h. Equivalently, $x_{k(\delta, \mathcal{S}_0)}^\delta$ is the best solution during that iterative process, based on \mathcal{S}_0 . However, $x_{k(\delta, \mathcal{S}_0)}^\delta$ may not be the most optimal solution during that iterative process, i.e., with the minimal MSE, but since x^\dagger is not known a-priori, the most optimal solution can not be estimated without additional knowledge.

In contrast, the classical (weaker) denoiser H_{σ_0} produce a significantly better result, as can be seen in Figure 2b. Again, the reasons being, (1st) it does not hallucinate features or impose structures on a learned basis and, (2nd) the (Fast) FBS-PnP algorithm updates the iterates x_k^δ gradually to fit the noisy data b_δ , i.e., noise in x_k^δ appears gradually, which then can be effectively denoised by H_{σ_0} , even if it's weak, without any hallucinations. However, H_{σ_0} will fail in the ADMM-PnP algorithm, if used naively, as shown in Example 3.2, since the noise intensities in the iterates x_k^δ (for ADMM-PnP algorithm) is very high, due to the large updates in the data-consistency steps towards the noisy data b_δ , and as H_{σ_0} is a weaker denoiser (for $\sigma_0 = 0.001$), it can not effectively denoise the noisy iterates x_k^δ , of high noise levels, to produce well-denoised iterates z_k^δ .

3.1. Subduing the instabilities/artifacts of a learned denoiser.

As explained in [20], we would like to introduce an additional attenuating-parameter $0 \leq \alpha \leq 1$ to attenuate the denoising strength of H_{θ_0} . This can be achieved by (externally) parameterizing H_{θ_0} to $H_{\theta_0, \alpha}$, where the denoiser $H_{\theta_0, \alpha}$ is defined as follows

$$\begin{aligned} H_{\theta_0, \alpha}(x_k^\delta) &:= x_k^\delta + \alpha (H_{\theta_0}(x_k^\delta) - x_k^\delta) \\ &= (1 - \alpha) x_k^\delta + \alpha H_{\theta_0}(x_k^\delta). \end{aligned} \quad (3.1)$$

Note that, with this transformation, the resulting (new) direction at any kth-step is given by, for the (new) denoised iterate $z_k^\delta(\alpha) := H_{\theta_0, \alpha}(x_k^\delta)$,

$$\begin{aligned} d_k^\delta(\alpha) &= z_k^\delta(\alpha) - z_{k-1}^\delta \\ &= (x_k^\delta - z_{k-1}^\delta) + \alpha (H_{\theta_0}(x_k^\delta) - x_k^\delta). \end{aligned} \quad (3.2)$$

Hence, if the denoising-to-consistency ratio $DC(k) \gg 1$ (very large), which can indicate over-denoising, then by opting a smaller α value ($\alpha \ll 1$), one can reduce the extent of denoising and can obtain a well-regularized solution. Table 1 shows the performance metrics of the recoveries, obtained using different values of α , and Figure 2 shows the corresponding recovered solutions. Figures 4a and 4b show the graph of denoising-to-consistency ratio ($DC(k, \alpha)$ vs. k), for different values of α , before and after attenuating the denoising strength of H_{θ_0} to $H_{\theta_0, \alpha}$. One can see that, the ratios $DC(k, \alpha)$ are quite high before attenuating the denoiser and are moderate after subduing it, indicating suitable denoising. However, for very small value of α , the ratio $DC(k, \alpha) \ll 1$, indicating inadequate denoising, which is also reflected in the recovery.

Example 3.2. [ADMM-PnP using H_{θ_0} vs. H_{σ_0}]

In this example, we compare the recoveries obtained in the ADMM-PnP algorithm, when using H_{θ_0} vs. H_{σ_0} . Here, we show that, unlike the previous example, using the (strong) denoiser H_{θ_0} leads to a much better recovery than using the classical (weak) denoiser H_{σ_0} , naively. The reason being, in an ADMM-PnP algorithm the data-consistency step (2.3) can be large, for smaller ρ values, resulting in x_k^δ having high noise intensities, and hence, can be appropriately denoised by a stronger denoiser H_{θ_0} . In contrast, here, the weaker denoiser H_{σ_0} , for small σ_0 , will yield a noisy reconstruction, since the data-denoising step is not strong enough to compensate the high noise levels arising in the iterates x_k^δ (from the large data-consistency step towards the noisy data b_δ), resulting in under-denoised iterates z_k^δ . Now, similar to attenuating a strong denoiser (via parameterizing it with an external attenuating parameter α), one can attempt to boost or augment the denoising strength of a weaker denoiser (via some form of parameterization) but, this is relatively much harder than the previous scenario, for reasons explained below.

Again, we keep the experimental settings of Example 3.1 unchanged, except, we implement the ADMM-PnP algorithm, instead of the FBS-PnP algorithm, using the learned denoiser H_{θ_0} and the classical denoiser H_{σ_0} . The numerical values of the results are shown in Table 2 and the figures in Figure 3. Note that, Figure 2a shows the recovered solution without any denoisers (x_N^δ after 250 CGLS iterations), Figure 3a shows $x_{k(\delta, S_0)}^\delta$, for $k(\delta, S_0) = 108$, using the learned denoiser H_{θ_0} and Figure 3b shows $x_{k(\delta, S_0)}^\delta$, for $k(\delta, S_0) = 3$, using the classical denoiser H_{σ_0} , where for inner optimization problem (2.3) we consider $\rho = 1$ and used 100 CGLS-iterations (with x_k^δ as the starting point). Here, one can see the improvements in the recovered solution using H_{θ_0} over H_{σ_0} , for reasons explained above.

3.2. Boosting a weak denoiser in ADMM-PnP.

In contrast to attenuating a strong denoiser, boosting a weaker denoiser is relatively much harder, since one cannot simply parameterize a weak denoiser, naively, by any external parameter $\alpha > 1$, like in (3.1). In [20], we provided a technique to boost a weaker denoiser when used in a FBS-PnP, as well as, ADMM-PnP settings. Here, we also provide certain insights to boost a weak denoiser in an ADMM-PnP setting, from a different angle. To have a better understanding of the reasons behind the boosting strategy, we would like to first dissect the net-change direction, at each step, in an ADMM-PnP algorithm. Note that, comparing the FBS-PnP algorithm to the ADMM-PnP algorithm, we have at every step k , fixing u_{k-1}^δ ,

$$z_{k-1}^\delta \mapsto x_k^\delta = \arg \min_x \mathcal{D}(x) + \rho \|x - (z_{k-1}^\delta - u_{k-1}^\delta)\|_2^2, \leftarrow \text{data-consistency step} \quad (3.3)$$

$$x_k^\delta \mapsto z_k^\delta = H_{\sigma_k}(x_k^\delta + u_{k-1}^\delta), \leftarrow \text{data-denoising step}, \quad (3.4)$$

and hence, the resulting direction, from z_{k-1}^δ to z_k^δ , is given by

$$\begin{aligned} d_{k-1}^\delta &:= z_k^\delta - z_{k-1}^\delta \quad (3.5) \\ &= \underbrace{\left[\arg \min_x \mathcal{D}(x) + \rho \|x - (z_{k-1}^\delta - u_{k-1}^\delta)\|_2^2 \right] - z_{k-1}^\delta}_{\text{data-consistency}} + \underbrace{\left[H_{\sigma_k}(x_k^\delta + u_{k-1}^\delta) - (x_k^\delta + u_{k-1}^\delta) \right]}_{\text{data-denoising}}. \end{aligned}$$

And, since one only estimates the minimizer of (3.3), through certain number of iterative optimization steps, the resulting direction is in fact dependent on the optimization architecture ($\mathcal{O}\mathcal{A}$), which includes the number of iterations (N), the initial iterates (y_0^k), the step-sizes τ'_k , as well as, the error-iterate u_{k-1}^δ i.e.,

$$d_{k-1}^\delta = d_{k-1}^\delta(z_{k-1}^\delta, x_k^\delta(\mathcal{O}\mathcal{A}(N, y_0^k, \tau'_k)), z_k^\delta(H_{\sigma_k}), u_{k-1}^\delta), \quad (3.6)$$

in comparison, the resulting direction in a FBS-PnP algorithm is simply dependent on the the step-size τ_k and the gradient $\nabla_x \mathcal{D}(z_{k-1}^\delta)$, i.e.,

$$d_{k-1}^\delta = d_{k-1}^\delta(z_{k-1}^\delta, x_k^\delta(\tau_k, \nabla_x \mathcal{D}(z_{k-1}^\delta)), z_k^\delta(H_{\sigma_k})). \quad (3.7)$$

Thus, one can see that for $u_{k-1}^\delta \equiv 0$, for all k , and $\mathcal{O}\mathcal{A}$ corresponding to a single step ($N = 1$) of the descent direction, starting from $y_0^k = z_{k-1}^\delta$ with $\tau'_k = \tau_k$, i.e., $x_k^\delta(\mathcal{O}\mathcal{A}(N, y_0^k, \tau'_k)) = z_{k-1}^\delta - \tau_k \nabla_x \mathcal{D}(z_{k-1}^\delta)$, we retrieve back the FBS-PnP algorithm. Hence, for $H_{\sigma_k} = H_{\sigma_0}$, for all k , and appropriately modifying the initial iterates (y_0^k) corresponding to Fast FBS-PnP algorithm, i.e., with a momentum step (3.10), we can significantly improve over the previously recovered ADMM-PnP solution. But then, one could have simply stuck with the Fast FBS-PnP algorithm, as we are not changing anything. In other words, we would like to investigate if there are other paths (descent flows) that can provide better results. Note that, the struggle faced by the weak denoiser H_{σ_0} , in this case, is that, it has to denoise $x_k^\delta + u_{k-1}^\delta$, where u_{k-1}^δ is the error term as defined in (2.5), and hence, unable to produce an effective denoised iterate $z_k^\delta = H_{\sigma_0}(x_k^\delta + u_{k-1}^\delta)$. Now, instead of forcing $u_k^\delta \equiv 0$, for all k , we can have a scaled error update, given by

$$u_{k+1}^\delta = u_k^\delta + \phi(x_{k+1}^\delta - z_{k+1}^\delta), \quad \leftarrow \text{scaled noise update step} \quad (3.8)$$

for $0 \leq \phi \leq 1$, which can also lead to efficient recoveries, see Table 2 and Figure 3. Therefore, one can observe that, the recovery in an ADMM-PnP algorithm (in fact, for any iterative regularization scheme, see [20]) is heavily dependent on the flow of the evolving iterations, even to an extent that, minimizing the expression in (3.3) with a different formulation:

$$x_k^\delta = \arg \min_x \frac{1}{\rho} \mathcal{D}(x) + \|x - (z_{k-1}^\delta - u_{k-1}^\delta)\|_2^2, \quad (3.9)$$

will also yield a different solution, as we are not completely minimizing them. For example, compare the results in Table 2 for $\text{GD}(N, \phi, \tau', y_0^k)$, which solves (3.9) for 10 iterations, vs. $\text{CGLS}(N, \phi, \rho, y_0^k)$, which solves (3.3) for 10 iterations, for the same ρ value. Some of the results corresponding to different $\mathcal{O}\mathcal{A}$ is presented in Table 2, where $\text{CGLS}(N, \phi, \rho, y_0^k)$ stands for conjugate-gradient least-squares method with N iterations, ϕ (u_k^δ scaling parameter, as in (3.8)), ρ (Lagrangian parameter) and y_0^k is the initial point for the inner optimization process, which can be x_k^δ , z_k^δ or y_k^δ , where y_k^δ is a momentum step given by, $y_0^\delta = z_0^\delta$ and for $k \geq 1$

$$y_k^\delta \mapsto y_k^\delta = y_k^\delta + \alpha_k(y_k^\delta - y_{k-1}^\delta), \quad \leftarrow \text{momentum-step} \quad (3.10)$$

with $\alpha_k = \frac{t_{k-1}-1}{t_k}$ and $t_k = \frac{(1+\sqrt{1+4t_{k-1}^2})}{2}$; and $\text{GD}(N, \phi, \tau', y_0^k)$ stands for the simple gradient descent method with a constant step-size (τ') and the gradient is defined as $-\tau' \nabla_x \mathcal{D}(x) - (x + (z_{k-1}^\delta - u_{k-1}^\delta))$. We can see, from Table 2, that when using $\text{GD}(N, \phi, \tau', y_0^k)$, for $\phi = 10^{-5}$, $\tau' = 10^{-5}$, $y_0^k = y_k^\delta$ and $N = 1$, we recover the best solution, even surpassing the Fast FBS-PnP solution. In contrast, the ADMM-PnP

performance using H_{θ_0} is degrading with smaller ϕ values, since we are moving closer the FBS-PnP algorithm. Furthermore, even the iterative flow corresponding to $\text{GD}(1, 10^{-5}, 10^{-5}, y_k^\delta)$, for which we got the best result, may not be the best solution flow, that is, one might even recover better solutions through different $\mathcal{O}\mathcal{A}$, ρ or ϕ values. Now, one may question the well-defineness of the recovered solution, since based on the same denoiser we are recovering wildly different solutions, where the answer to this question is explained in [20]. Note that, similar to Example 3.1, we can also plot the denoising-to-consistency ratio $DC(k)$ over the iterations, for the different denoisers and their $\mathcal{O}\mathcal{A}$, ρ and ϕ values, some of which are shown in Figure 5. One can see that, the $\mathcal{O}\mathcal{A}$, ρ and ϕ values for which $DC(k)$ is small, yields a noisy solution, where as, the $\mathcal{O}\mathcal{A}$, ρ and ϕ values associated with large $DC(k)$, results in a well-denoised reconstruction.

Example 3.3. [FBS-PnP using H_{θ_0} and H_{σ_0} together]

In this example, we combine the denoisers H_{θ_0} and H_{σ_0} together, to produce the denoised iterates z_k^δ and examine their joined effects, i.e., we would like to take advantage of both these denoisers, the classical as well as the learned. Again, we keep the experimental setup of Example 3.1 unchanged, but use the following weighted denoiser, for $\alpha \geq 0$ and $\beta \geq 0$,

$$H_{\alpha\theta_0+\beta\sigma_0} = \alpha H_{\theta_0} + \beta H_{\sigma_0} \quad (3.11)$$

in the FBS-PnP algorithm. First, we try with assigning equal weights ($\alpha = \beta = \frac{1}{2}$), i.e., $H_{(\theta_0+\sigma_0)/2} = (H_{\theta_0} + H_{\sigma_0})/2$, and the results are shown in Table 3 and Figure 7. Although it's better than using only H_{θ_0} , but no where comparable to the result obtained using H_{σ_0} , since the strong denoiser H_{θ_0} is dominating. Of course, now one can subdue the denoiser $H_{(\theta_0+\sigma_0)/2}$, as done for H_{θ_0} in (3.1), but then, we won't be making much use of H_{σ_0} . The proper usage of both these denoisers is through weighing them differently in (3.11). We instead use a simpler (normalized) version of the expression shown in (3.11), by having $\beta = 1 - \alpha$, for $0 \leq \alpha \leq 1$, i.e.,

$$H_{\alpha H_{\theta_0}+(1-\alpha)H_{\sigma_0}} = \alpha H_{\theta_0} + (1 - \alpha)H_{\sigma_0}. \quad (3.12)$$

The recoveries corresponding to few α values are presented in Table 3 and Figure 7. In addition, note that, the simpler expression in (3.12) further helps us to automate the selection of the α -values, via a method suggested in [20], that is, at every step k , choose the value of α such that $z_k^\delta(\alpha) = H_{\alpha H_{\theta_0}+(1-\alpha)H_{\sigma_0}}(x_k^\delta)$ best satisfies the selection criterion \mathcal{S} , i.e.,

$$\alpha_0(k) := \arg \min_{\alpha \in [0,1]} \mathcal{S}(z_k^\delta(\alpha)) \quad (3.13)$$

$$\text{such that, } z_k^\delta(\alpha) := H_{\alpha H_{\theta_0}+(1-\alpha)H_{\sigma_0}}(x_k^\delta) = \alpha H_{\theta_0}(x_k^\delta) + (1 - \alpha)H_{\sigma_0}(x_k^\delta).$$

Note that, the minimization problem (3.13) may not be strictly convex, i.e., there might not be a global minimizer $\alpha_0(k)$. Nevertheless, this is simply a sub-problem intended to find an appropriate α value between 0 and 1, depending on the selection criterion \mathcal{S} , and hence, even if the best α_0 is not obtained, any $\alpha \in [0,1]$ will reduce the denoising strength, and empirical results show that (3.13) works fine, see Figure 7 and Table 3. Moreover, one doesn't have to compute $H_{\theta_0}(x_k^\delta)$ and $H_{\sigma_0}(x_k^\delta)$ repeatedly for different values of α , when finding α_0 in (3.13), as it can be expensive; one simply has to compute them once, for each iterations iteration, and use the results $(H_{\theta_0}(x_k^\delta), H_{\sigma_0}(x_k^\delta))$ to find $\alpha_0(k)$. Note that, from Figure 7g, the values of $\alpha_0(k)$ are high initially but then it's almost zero in the later iterations,

indicating that H_{θ_0} is active in the initial iterations but then its contribution is pushed to zero (to avoid any instabilities/hallucinations arising from it), and the contribution of H_{σ_0} starts dominating. This even leads to a recovery better than using only H_{σ_0} . Also, from the $DC(k, \alpha)$ ratio graph in Figure 6, one can observe that, for equal weights ($\alpha = \beta$) the ratio $DC(k)$ keeps on increasing (as H_{θ_0} is dominant), where as, the graph does not blow up for $\alpha_0(k)$, generated from (3.13).

Example 3.4. In this example, keeping the settings of Example 3.1 unchanged, we perform the ADMM-PnP algorithm using the weighted combination of both the denoisers H_{θ_0} and H_{σ} , i.e., $H_{\alpha H_{\theta_0} + (1-\alpha)H_{\sigma_0}}$, for $\alpha \in [0, 1]$, as defined in (3.12). Note that, here the optimization architecture ($\mathcal{O}\mathcal{A}$), for solving the data-consistency step (3.9), and the value of ϕ also effect the recovery process. Thus, one can observe that, for $\mathcal{O}\mathcal{A}$ and ϕ values that promote larger data-consistency steps, such as $\text{CGLS}(N, \phi, \rho, y_0^k)$ for large N , ϕ values and small ρ value (i.e., the noise levels in x_k^δ increase rapidly), if we choose α based on (3.13), then the weighted denoiser $H_{\alpha_0 H_{\theta_0} + (1-\alpha_0)H_{\sigma_0}}$ behaves similar to H_{θ_0} (i.e., $\alpha_0 \approx 1$), since H_{θ_0} can denoise x_k^δ more appropriately and H_{σ_0} is inefficient, in this case. In contrast, for $\mathcal{O}\mathcal{A}$ and ϕ values that promote smaller data-consistency steps, such as $\text{GD}(N, \phi, \tau', y_0^k)$ for small N , τ' and ϕ values (i.e., the noise levels in x_k^δ increase steadily), if we choose α based on (3.13), then the stronger denoiser H_{θ_0} is dominant for the initial few iterations, when the noise level is high, but for later iterations, the contribution of H_{σ_0} dominates H_{θ_0} (i.e., $\alpha_0(k) \approx 1$, for initial few k , and $\alpha_0(k) \approx 0$, for $k \gg 1$), to avoid the instabilities/hallucinations created from H_{θ_0} , in this case. This is also true for any fixed value of α , i.e., if $\mathcal{O}\mathcal{A}$ promotes fast increment in the noise levels of x_k^δ , then larger value of α (i.e., H_{θ_0} dominating H_{σ_0}) provides better result than smaller α -values, where as, if $\mathcal{O}\mathcal{A}$ promotes slow increment in the noise levels of x_k^δ , then smaller value of α (i.e., H_{σ_0} dominating H_{θ_0}) provides better result than smaller α -values. These phenomena are presented in Table 4 and Figure 7.

4. CONCLUSION AND FUTURE RESEARCH

In this paper, we tried to present the instabilities/hallucinations arising in a PnP-algorithm when using a learned denoiser, which can be quite different from the artifacts/instabilities inherent to an inverse problem. We then provide some techniques to subdue these instabilities, produce stable reconstructions and improve the recoveries significantly. We also compare the behavior/dynamics of the FBS-PnP algorithm vs. the ADMM-PnP algorithm, and which method produce better results, depending on a given scenario. In fact, we showed that the ADMM-PnP algorithm is heavily dependent on the optimization architecture ($\mathcal{O}\mathcal{A}$), involved in the data-consistency step, and the recoveries can greatly improve/degrade depending on $\mathcal{O}\mathcal{A}$ and the ϕ values. In addition, we also present a method to combine the classical denoiser and the learned denoiser, in a weighted manner, to produce results, which are much better than the individual reconstructions, i.e., one can take advantage of both these worlds.

In a future work, we would like to extend this idea to apply on image reconstruction methods based on deep-learning, i.e., instead of using a learned denoiser in the PnP-algorithm, the image reconstruction methods that involve deep-learning architecture directly in the reconstruction process, such as an unrolled neural network scheme for image reconstruction. We believe that, by incorporating ideas similar

to what is developed in this paper, one can also subdue the instabilities arising in those methods, as is shown in [21].

Comparing denoisers $H_{\theta_0, \alpha}$ (Attenuated DnCNN) vs. H_{σ_0} (BM3D)							
$H_{\theta_0, \alpha}$	$k(\delta, \mathcal{S}_0)$	MSE	\mathcal{D} -err.	\mathcal{S} -err.	PSNR	SSIM	Min.MSE
$\alpha = 1$	47	0.3848	0.0667	0.0745	20.46	0.4493	0.3608 (40)
$\alpha = 0.1$	81	0.1796	0.0219	0.0236	27.08	0.8004	0.1763 (74)
$\alpha = 0.01$	140	0.1241	0.0096	0.0150	30.29	0.7899	0.1231 (154)
$\alpha = 0.001$	250	0.1151	0.0058	0.0153	30.95	0.6901	0.1151 (250)
$\alpha = 0.0001$	250	0.1800	0.0048	0.0202	27.06	0.4579	0.1800 (250)
H_{σ_0}	250	0.0450	0.0101	0.0099	39.09	0.9340	0.0450 (250)

TABLE 1. FBS-PnP: learned vs. classical denoiser, Example 3.1.

REFERENCES

- [1] H. W. Engl, M. Hanke, and A. Neubauer, *Regularization of inverse problems*, vol. 375 of *Mathematics and its Applications*. Kluwer Academic Publishers Group, Dordrecht, 1996.
- [2] A. Bakushinsky and A. Goncharky, *Ill-posed problems: theory and applications*, vol. 301 of *Mathematics and its Applications*. Kluwer Academic Publishers Group, Dordrecht, 1994. Translated from the Russian by I. V. Kochikov.
- [3] C. W. Groetsch, *The theory of Tikhonov regularization for Fredholm equations of the first kind*, vol. 105 of *Research Notes in Mathematics*. Pitman (Advanced Publishing Program), Boston, MA, 1984.
- [4] J. Baumeister, *Stable solution of inverse problems*. Advanced Lectures in Mathematics, Friedr. Vieweg & Sohn, Braunschweig, 1987.
- [5] V. A. Morozov, *Methods for solving incorrectly posed problems*. Springer-Verlag, New York, 1984. Translated from the Russian by A. B. Aries, Translation edited by Z. Nashed.
- [6] M. Hanke, “Accelerated landweber iterations for the solution of ill-posed equations,” *Numerische Mathematik*, vol. 60, pp. 341–373, Dec 1991.
- [7] L. Landweber, “An iteration formula for fredholm integral equations of the first kind,” *American Journal of Mathematics*, vol. 73, no. 3, pp. 615–624, 1951.
- [8] M. Hanke, A. Neubauer, and O. Scherzer, “A convergence analysis of the landweber iteration for nonlinear ill-posed problems,” *Numerische Mathematik*, vol. 72, pp. 21–37, Nov 1995.
- [9] A. Beck and M. Teboulle, “A fast iterative shrinkage-thresholding algorithm for linear inverse problems,” *SIAM J. Imaging Sciences*, vol. 2, pp. 183–202, 01 2009.
- [10] S. Boyd, N. Parikh, E. Chu, B. Peleato, and J. Eckstein, “Distributed optimization and statistical learning via the alternating direction method of multipliers,” *Found. Trends Mach. Learn.*, vol. 3, p. 1–122, Jan. 2011.
- [11] A. Chambolle and T. Pock, “A first-order primal-dual algorithm for convex problems with applications to imaging,” *Journal of Mathematical Imaging and Vision*, vol. 40, no. 1, pp. 120–145, 2011.
- [12] S. V. Venkatakrisnan, C. A. Bouman, and B. Wohlberg, “Plug-and-play priors for model based reconstruction,” in *2013 IEEE Global Conference on Signal and Information Processing*, pp. 945–948, 2013.
- [13] S. H. Chan, X. Wang, and O. A. Elgendy, “Plug-and-play admm for image restoration: Fixed-point convergence and applications,” *IEEE Transactions on Computational Imaging*, vol. 3, no. 1, pp. 84–98, 2017.
- [14] G. T. Buzzard, S. H. Chan, S. Sreehari, and C. A. Bouman, “Plug-and-play unplugged: Optimization-free reconstruction using consensus equilibrium,” *SIAM Journal on Imaging Sciences*, vol. 11, no. 3, pp. 2001–2020, 2018.
- [15] E. Ryu, J. Liu, S. Wang, X. Chen, Z. Wang, and W. Yin, “Plug-and-play methods provably converge with properly trained denoisers,” in *Proceedings of the 36th International Conference on Machine Learning* (K. Chaudhuri and R. Salakhutdinov, eds.), vol. 97 of *Proceedings of Machine Learning Research*, pp. 5546–5557, PMLR, 09–15 Jun 2019.

Comparing denoisers $H_{\theta_0, \alpha}$ vs. H_{σ_0} (BM3D), for various $\mathcal{O}\mathcal{A}(N, \phi, \rho, \tau', y_0^k)$							
CGLS (N, ϕ, ρ, y_0^k)	N = 100	$\phi = 1$	$\rho = 1$	$y_0^k =$ x_k^δ			
Denoiser	$k(\delta, \mathcal{S}_0)$	MSE	\mathcal{D} -err.	\mathcal{S} -err.	PSNR	SSIM	Min.MSE
H_{θ_0}	108	0.1200	0.0045	0.0171	30.59	0.5878	0.1168 (15)
H_{σ_0}	3	0.2184	0.0045	0.0243	25.38	0.3805	0.2177 (2)
Fixing H_{θ_0} ,	fix	ϕ	y_0^k	but	$\rho,$	N	changing
N=10/ ρ =1	182	0.1203	0.0046	0.0171	30.57	0.5861	0.1201 (239)
N=10/ ρ =100	240	0.0934	0.0083	0.0129	32.77	0.8803	0.0933 (49)
N=100/ ρ =100	217	0.0934	0.0083	0.0129	32.77	0.8803	0.0933 (17)
Fixing H_{σ_0} ,	fix	ϕ	y_0^k	but	$\rho,$	N	changing
N=10/ ρ =1	20	0.2197	0.0044	0.0243	25.33	0.3759	0.2141 (11)
N=10/ ρ =100	31	0.2201	0.0044	0.0243	25.32	0.3744	0.2139 (14)
N=100/ ρ =100	15	0.2209	0.0044	0.0243	25.29	0.3721	0.2138 (6)
GD (N, ϕ, τ', y_0^k)	fix	H_{θ_0}	N= 10	$\tau' =$ 10^{-5}	$y_0^k =$ y_k^δ	but	changing ϕ
$\phi = 10^{-1}$	22	0.1723	0.0197	0.0237	27.44	0.8026	0.1719 (21)
$\phi = 10^{-3}$	21	0.1960	0.0252	0.0277	26.32	0.7596	0.1926 (19)
$\phi = 10^{-5}$	21	0.1964	0.0254	0.0278	26.31	0.7583	0.1929 (19)
GD (N, ϕ, τ', y_0^k)	fix	H_{σ_0}	N= 10	$\tau' =$ 10^{-5}	$y_0^k =$ y_k^δ	but	changing ϕ
$\phi = 10^{-1}$	84	0.2219	0.0045	0.0248	25.24	0.3674	0.2166 (52)
$\phi = 10^{-3}$	250	0.1497	0.0050	0.0162	28.67	0.5857	0.1473 (209)
$\phi = 10^{-5}$	250	0.1405	0.0051	0.0158	29.21	0.6008	0.1400 (229)
CGLS (N, ϕ, ρ, y_0^k)	fix	H_{σ_0}	N= 10	$\rho =$ 10^5	$y_0^k =$ y_k^δ	but	changing ϕ
$\phi = 10^{-3}$	250	0.2850	0.0384	0.0525	23.07	0.7222	0.2850 (250)
$\phi = 10^{-5}$	250	0.2850	0.0384	0.0525	23.07	0.7222	0.2850 (250)
GD (N, ϕ, τ', y_0^k)	fix	H_{σ_0}	$\phi =$ 10^{-5}	$\tau' =$ 10^{-5}	$y_0^k =$ y_k^δ	but	changing N
N = 100	25	0.2161	0.0045	0.0238	25.47	0.3846	0.2132 (17)
N = 10	250	0.1405	0.0051	0.0158	29.21	0.6008	0.1400 (229)
N = 3	250	0.0509	0.0093	0.0102	38.03	0.8992	0.0509 (250)
N = 1	250	0.0395	0.0102	0.0101	40.24	0.9640	0.0395 (250)

TABLE 2. ADMM-PnP: learned vs. classical denoiser, Example 3.2.

- [16] A. M. Teodoro, J. M. Bioucas-Dias, and M. A. T. Figueiredo, "A convergent image fusion algorithm using scene-adapted gaussian-mixture-based denoising," *IEEE Transactions on Image Processing*, vol. 28, no. 1, pp. 451–463, 2019.
- [17] Y. Sun, B. E. Wohlberg, and U. Kamilov, "An online plug-and-play algorithm for regularized image reconstruction," *IEEE Transactions on Computational Imaging*, vol. 5, 1 2019.
- [18] Y. Romano, M. Elad, and P. Milanfar, "The little engine that could: Regularization by denoising (red)," *SIAM Journal on Imaging Sciences*, vol. 10, no. 4, pp. 1804–1844, 2017.
- [19] J. Liu, Y. Sun, C. Eldeniz, W. Gan, H. An, and U. S. Kamilov, "Rare: Image reconstruction using deep priors learned without groundtruth," *IEEE Journal of Selected Topics in Signal Processing*, vol. 14, no. 6, pp. 1088–1099, 2020.

FBS-PnP: $x_{k(\delta, \mathcal{S}_0)}$ for $H_{\alpha\theta_0 + (1-\alpha)H_{\sigma_0}} = \alpha H_{\theta_0} + (1-\alpha)H_{\sigma_0}$							
α	$k(\delta, \mathcal{S}_0)$	MSE	\mathcal{D} -err.	\mathcal{S} -err.	PSNR	SSIM	Min.MSE
$\alpha=1 (H_{\theta_0})$	47	0.3848	0.0667	0.0745	20.46	0.4493	0.3608 (40)
$\alpha = 0.5$	53	0.2618	0.0432	0.0476	23.81	0.6131	0.2609 (51)
$\alpha = 0.1$	84	0.1757	0.0229	0.0218	27.27	0.8605	0.1709 (76)
$\alpha = 0.01$	141	0.0954	0.0123	0.0127	32.58	0.9531	0.0953 (139)
$\alpha=0 (H_{\sigma_0})$	250	0.0450	0.0101	0.0099	39.09	0.9340	0.0450 (250)
$\alpha = \alpha_0$	239	0.0398	0.0102	0.0099	40.16	40.16	0.0391 (250)

TABLE 3. Combining classical and learned denoiser, see Example 3.3.

ADMM-PnP: $x_{k(\delta, \mathcal{S}_0)}$ for $H_{\alpha\theta_0 + (1-\alpha)H_{\sigma_0}} = \alpha H_{\theta_0} + (1-\alpha)H_{\sigma_0}$							
CGLS (N, ϕ, ρ, y_0^k)	N = 10	$\phi = 1$	$\rho = 1$	$y_0^k =$ x_k^δ			
α	$k(\delta, \mathcal{S}_0)$	MSE	\mathcal{D} -err.	\mathcal{S} -err.	PSNR	SSIM	Min.MSE
$\alpha = 1 (H_{\theta_0})$	182	0.1203	0.0046	0.0171	30.57	0.5861	0.1201 (239)
$\alpha = 0 (H_{\sigma_0})$	20	0.2197	0.0044	0.0243	25.33	0.3759	0.2141 (11)
$\alpha = 0.5$	25	0.2145	0.0043	0.0234	25.54	0.3774	0.2112 (14)
$\alpha = 0.9$	92	0.1312	0.0043	0.0187	29.38	0.5257	0.1312 (250)
$\alpha = \alpha_0$	179	0.1202	0.0049	0.0171	30.57	0.5862	0.1201 (246)
GD (N, ϕ, τ', y_0^k)	N= 10	$\phi =$ 10^{-5}	$\tau' =$ 10^{-5}	$y_0^k =$ y_k^δ			
$\alpha = 1 (H_{\theta_0})$	21	0.1964	0.0254	0.0278	26.31	0.7583	0.1929 (19)
$\alpha = 0 (H_{\sigma_0})$	250	0.1405	0.0051	0.0158	29.21	0.6008	0.1400 (229)
$\alpha = 0.5$	24	0.1697	0.0197	0.0221	27.58	0.8249	0.1693 (23)
$\alpha = 0.9$	93	0.1307	0.0177	0.0154	29.84	0.8688	0.1284 (39)
$\alpha = \alpha_0$	217	0.0949	0.0087	0.0127	32.62	0.8998	0.0946 (212)

TABLE 4. Combining classical and learned denoiser, see Example 3.4.

- [20] A. Nayak, “Interpretation of plug-and-play (pnp) algorithms from a different angle,” 2021.
- [21] V. Antun, F. Renna, C. Poon, B. Adcock, and A. C. Hansen, “On instabilities of deep learning in image reconstruction and the potential costs of ai,” *Proceedings of the National Academy of Sciences*, vol. 117, no. 48, pp. 30088–30095, 2020.
- [22] Y. Mäkinen, L. Azzari, and A. Foi, “Exact transform-domain noise variance for collaborative filtering of stationary correlated noise,” in *2019 IEEE International Conference on Image Processing (ICIP)*, pp. 185–189, 2019.
- [23] Y. Mäkinen, L. Azzari, and A. Foi, “Collaborative filtering of correlated noise: Exact transform-domain variance for improved shrinkage and patch matching,” *IEEE Transactions on Image Processing*, vol. 29, pp. 8339–8354, 2020.
- [24] S. Gazzola, P. Hansen, and J. Nagy, “Ir tools - a matlab package of iterative regularization methods and large-scale test problems,” *Numerical Algorithms*, 2018.

VISITING ASSISTANT PROFESSOR, DEPARTMENT OF MATHEMATICS, UNIVERSITY OF ALABAMA AT BIRMINGHAM, UNIVERSITY HALL, ROOM 4005, 1402 10TH AVENUE SOUTH, BIRMINGHAM AL 35294-1241, (P) 205.934.2154, (F) 205.934.9025

Email address: nash101@uab.edu; avinashnike01@gmail.com

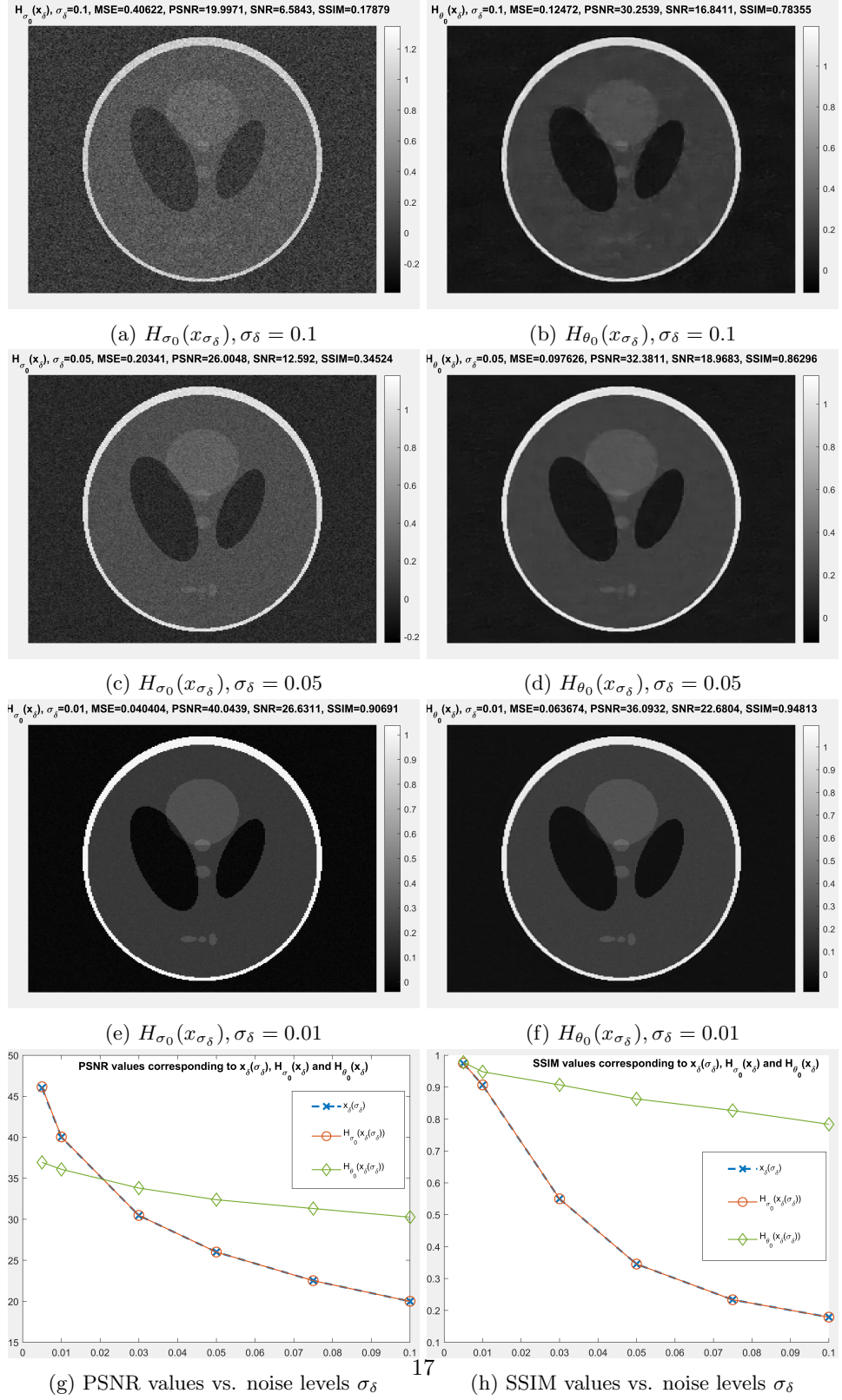


FIGURE 1. Comparing denoising strength of H_{θ_0} vs. H_{σ_0} .

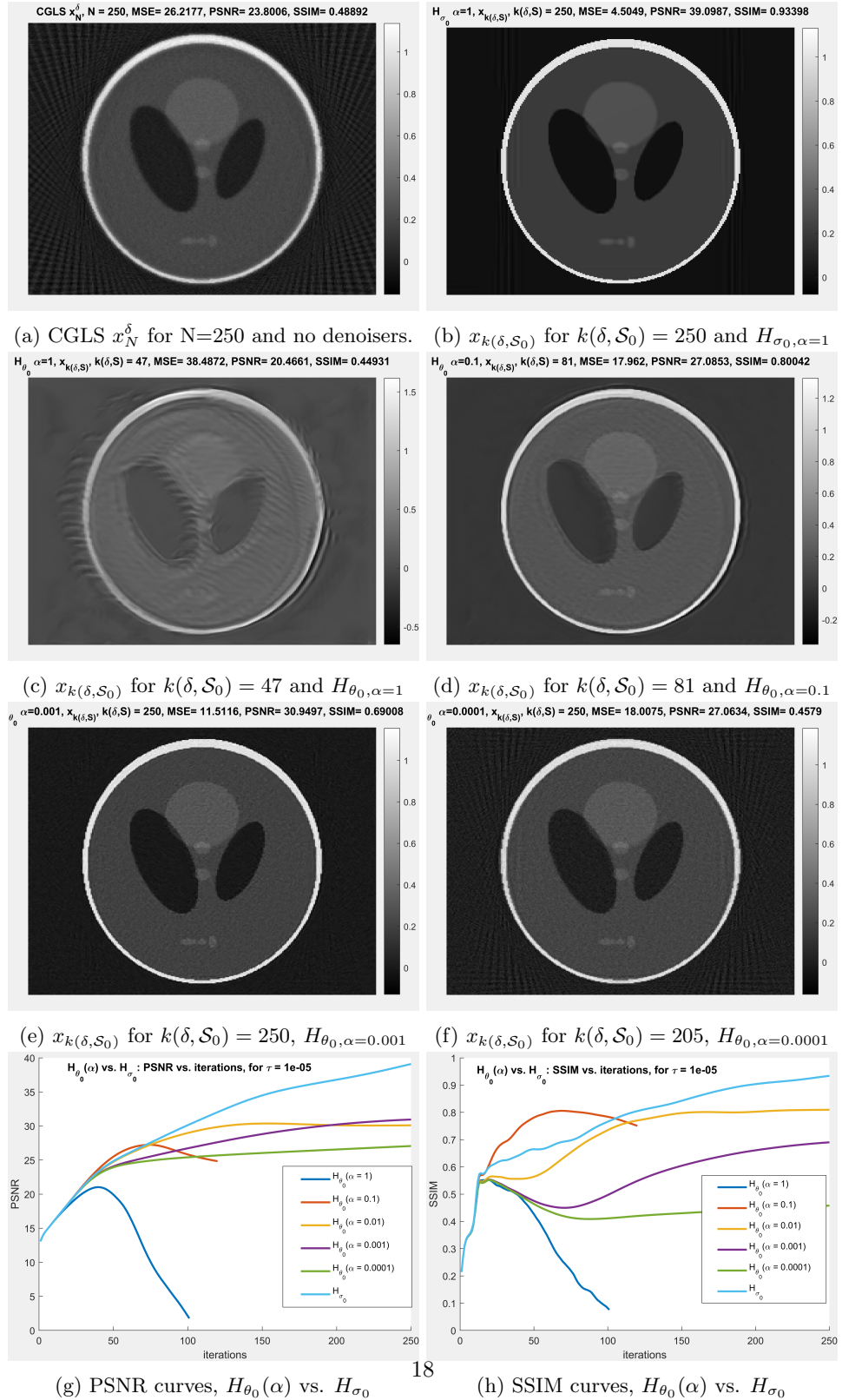


FIGURE 2. FBS-PnP: denoiser $H_{\theta_0}(\alpha)$ vs. H_{σ_0} , see Example 3.1.

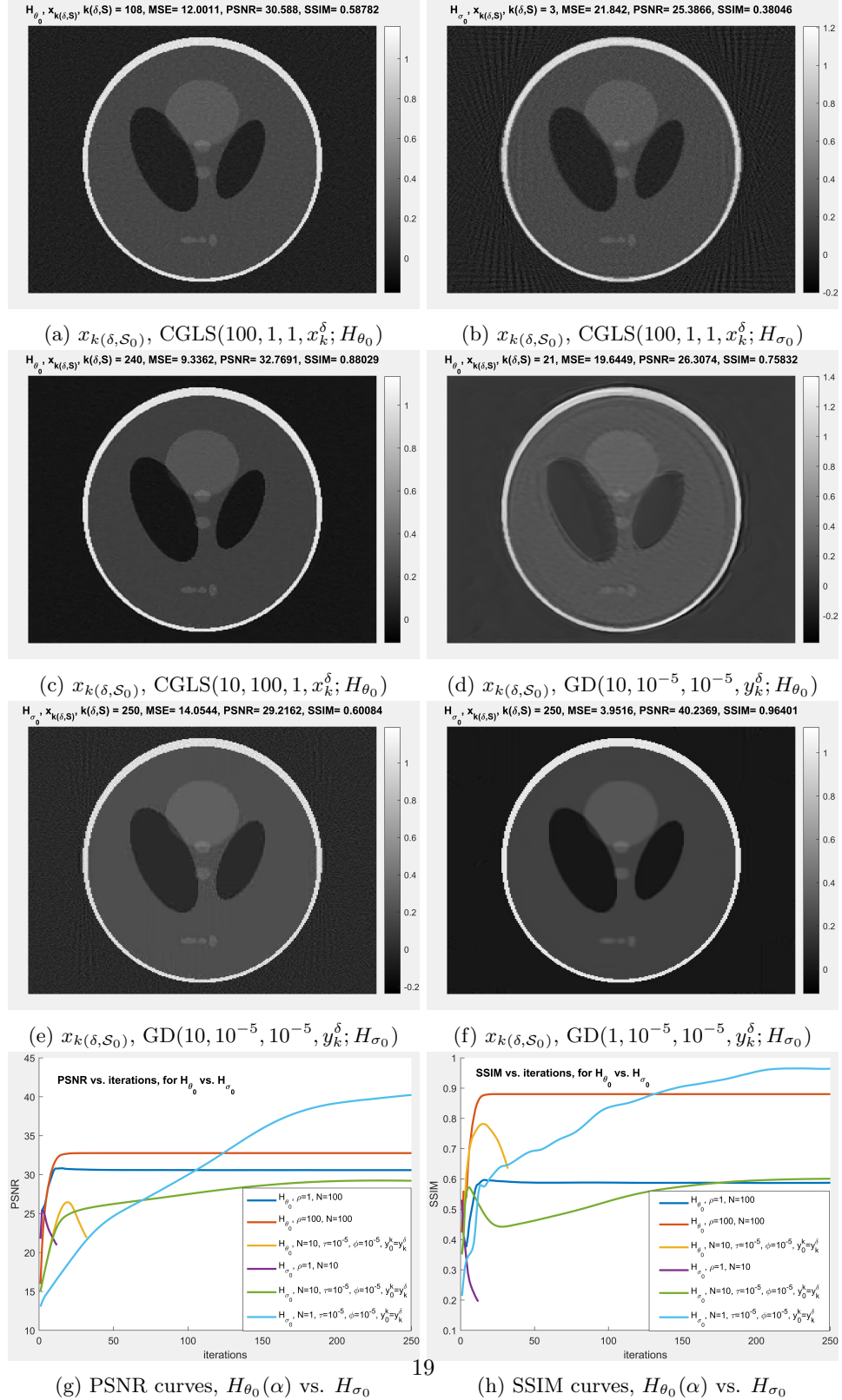


FIGURE 3. ADMM-PnP: denoiser $H_{\theta_0}(\alpha)$ vs. H_{σ_0} , see Example 3.2.

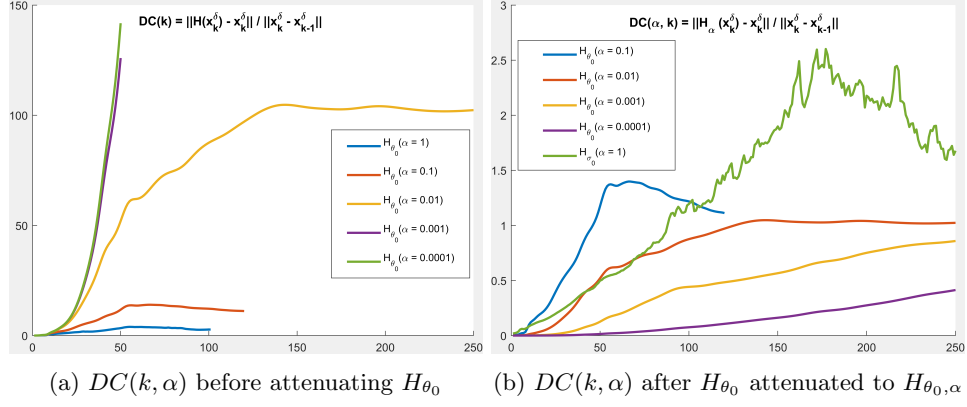


FIGURE 4. Denoising-to-consistency ratio ($DC(k)$), for Example 3.1.

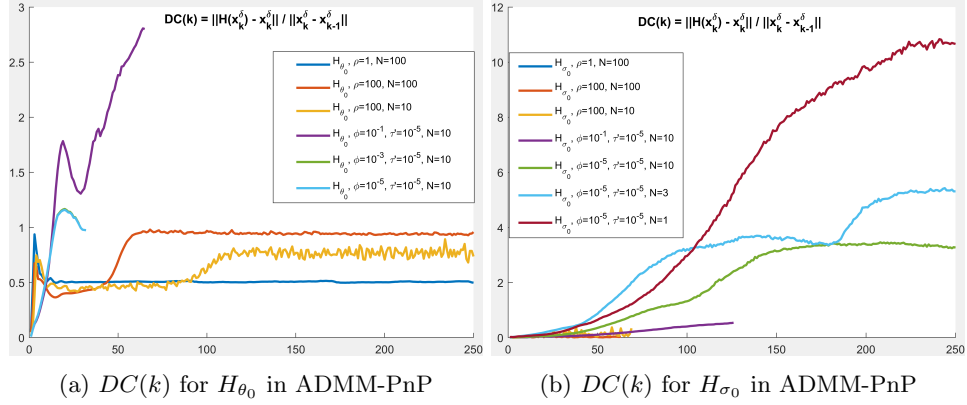


FIGURE 5. $DC(k)$ for different $\mathcal{O.A}$ in ADMM-PnP, see Example 3.2.

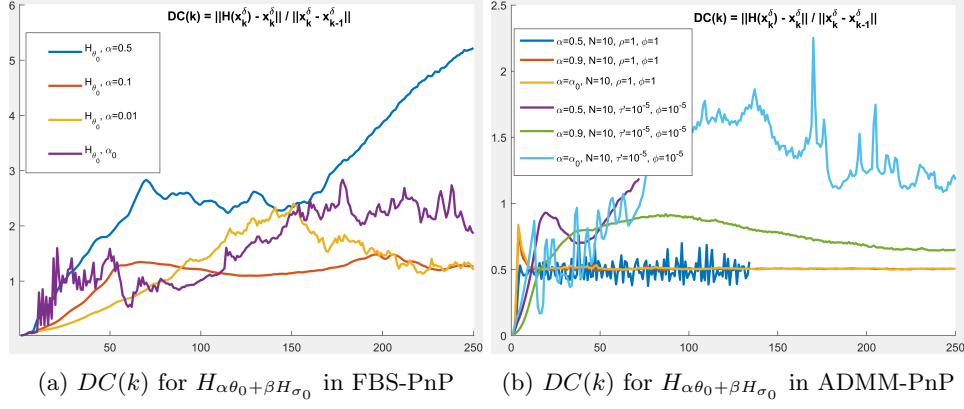


FIGURE 6. $DC(k)$ for $H_{\alpha\theta_0+\beta H_{\sigma_0}}$, such that $\alpha + \beta = 1$, in FBS-PnP vs. ADMM-PnP (with different $\mathcal{O}\mathcal{A}$ and ϕ values), see Example 3.3 and Example 3.4.

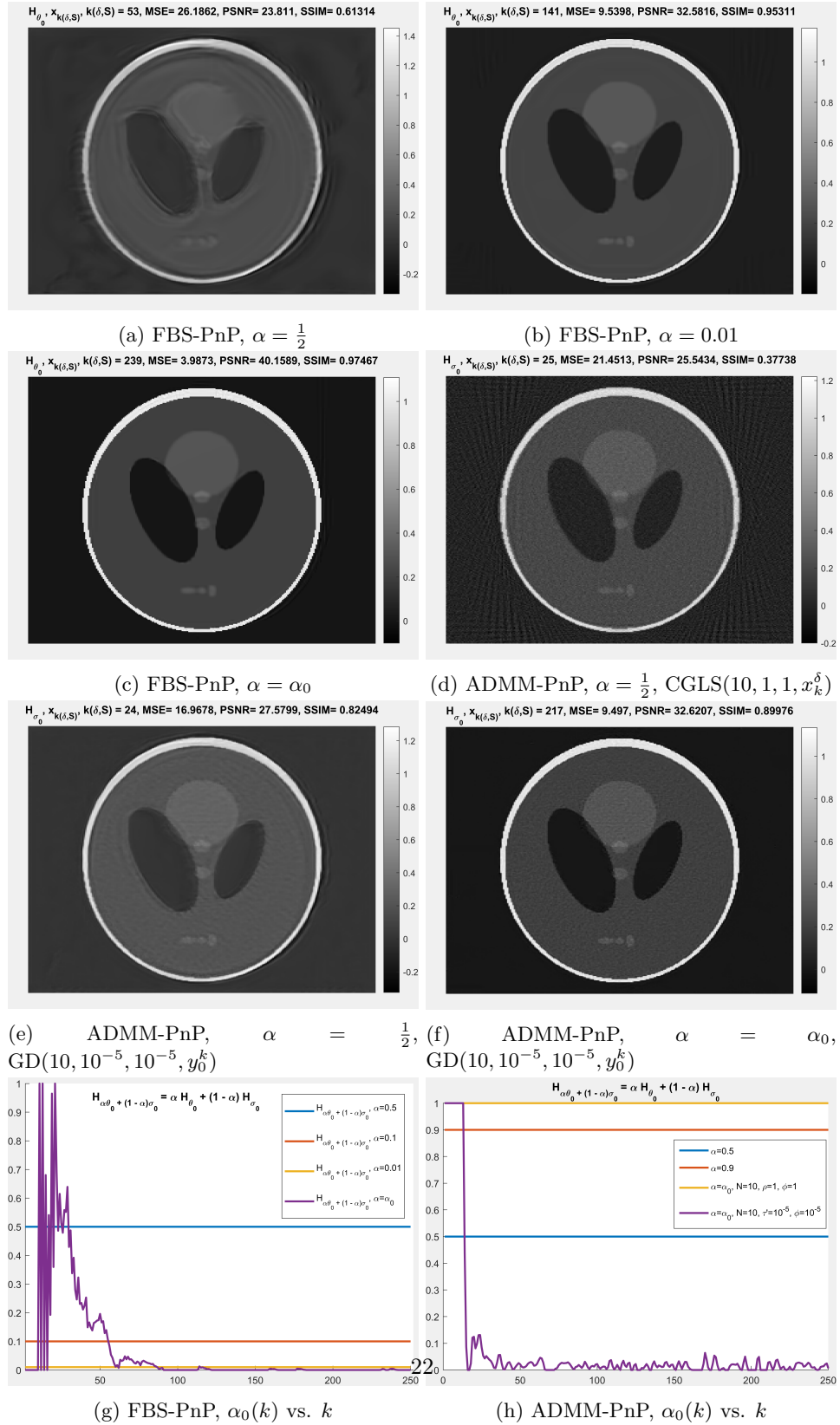


FIGURE 7. FBS-PnP and ADMM-PnP with $H_{\alpha\theta_0} + (1-\alpha)\sigma_0$, see Example 3.3 and Example 3.4